THE JOURNAL OF PHYSICAL CHEMISTRY C

Article

pubs.acs.org/JPCC

Heat Transfer at Solid−Gas Interfaces by Photoacoustics at Brillouin Frequencies

Chang-Ki Min, Kejia Chen, Sung Chul Bae, David G. Cahill,* and Steve Granick

Department of Materials Science and Engineering, and Materials Research Laboratory, University of Illinois, Urbana, Illinois 61801, United States

ABSTRACT: We use time-resolved ellipsometry to investigate the rate of heat transfer at solid−gas interfaces through measurements of the amplitude and phase of acoustic waves at Brillouin frequencies, 100−400 MHz, at pressures 2 orders of magnitude higher than earlier comparable studies. An ultrafast optical pulse heats a thin metal film deposited on a sapphire substrate. Heat flow from the substrate into the gas causes expansion of the gas and generates an acoustic wave that is probed by off-null ellipsometry with subpicosecond time resolution. We compare the amplitudes and phases of photoacoustic signals generated in inert gases Ne, Ar, Kr, and Xe to a continuum theoretical model that includes the thermal accommodation coefficient α at the gas−solid interface. For the surfaces we have studied, bare Au and Au coated by a self-assembled monolayer of 1-octadecanethiol (ODT), this comparison between experiment and theory for the amplitude of the photoacoustic waves suggests that α values for bare and ODT-terminated Au are similar and $\alpha > 0.3$. This conclusion is tentative, however, because the phases of the photoacoustic waves show systematic differences that are not predicted by the model. For tetrafluoroethane vapor (R-134a refrigerant), the photoacoustic signal generated by a Au surface coated with a hydrophilic (COOH-terminated) self-assembled monolayer is a factor of 2 larger than the photoacoustic signal generated by a hydrophobic (CH_3-terminated) monolayer. We also report measurements of the ultrafast ellipsometry signals generated by the sudden desorption of physisorbed methanol and water on hydrophobic and hydrophilic self-assembled monolayers.

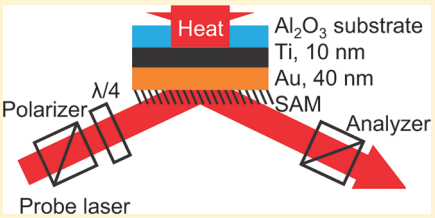

I. INTRODUCTION

The exchange of energy between an impinging gas molecule and a solid surface is a fundamental process that underlies a wide range of physical and chemical phenomena: condensation/evaporation,[1] atmospheric chemistry,[2] evolution of interstellar clouds of gas and dust,[3] and heat dissipation in nanowire electronics.[4,5] If the distribution of translation, rotational, and vibrational states of gas molecules can be described by a temperature T_g that is not too far removed from the temperature of a solid surface T_s, then this exchange of energy can be characterized by a thermal accommodation coefficient

$$\alpha = \frac{T_{g,o} - T_g}{T_s - T_g} \quad (1)$$

where $T_{g,o}$ is the effective temperature of "outgoing" molecules after interactions with the surface.[6−8]

Investigations of thermal accommodation date back to the foundations of surface science and were typically accomplished by measuring the rate of heat transfer between a small diameter metal filament and a low pressure gas. Almost 80 years ago, Blodgett and Langmuir[6] described how the thermal accommodation of H_2 could be used to probe the surface physical chemistry of a heated W filament. In general, the contribution of surface processes to the thermal resistance is measurable only when the characteristic length scale of the experiment approaches the mean-free path of the molecules in the gas, i.e., when the Knudsen number is not small compared to unity. In a conventional hot filament experiment, this requirement means that the diameter of the wire must be comparable to, or smaller than, the mean-free path; a typical wire diameter of 100 μm therefore limits the accessible pressure range to $P < 0.01$ atm.

The exchange of kinetic energy at the surface can also be measured directly in beam scattering experiments, and the scientific literature for scattering studies of clean metal surfaces in ultrahigh vacuum is extensive.[9−12] Scattering methods have also been applied to the surfaces of low-vapor-pressure liquids[13] and self-assembled organic monolayers.[14−18] Much insight can be gained from these detailed studies of gas-surface dynamics. In so-called "trapping desorption", a large fraction of the kinetic energy of an incident atom or molecule is accommodated by the surface. Typically, a match between the mass of the incident atom and the surface atoms facilitates the exchange of kinetic energy. A low-rigidity coating such as a self-assembled monolayer also tends to increase accommodation. In principle, the thermal accommodation, α in eq 1, could be evaluated from detailed knowledge of the energy and angle distribution of scattered molecules measured as a function of incident angle and incident energy for energies on the order of $2k_BT$. We also note that scattering experiments are limited to low pressures where the mean-free paths of the gas molecules are long and molecules travel ballistically between source and sample and sample and detector.

Here we describe an experimental method with sensitivity to heat transfer at interfaces between solids and gases at pressures

Received: October 26, 2011
Published: April 26, 2012

on the order of 1 atm because the characteristic length scale of the measurement, the periodicity of the sensitivity function of the ellipsometer, is ~1 μm. We use ultrafast pump−probe optical methods to detect high-frequency acoustic waves generated in the gas by the sudden heating and rapid cooling of a thin metal film.[19] Ellipsometry, i.e., measurements of the relative phase of the reflection coefficients of $\hat{p}$ and $\hat{s}$ polarized light, provides a high sensitivity measurement of the amplitude and phase of the acoustic waves.

II. GENERATION OF ACOUSTIC WAVES BY A RAPIDLY HEATED SURFACE

The experiment takes place in the time domain: a pump optical pulse heats a thin metal film deposited on a sapphire substrate; heat transfers into the gas and causes the gas to expand; and this expansion launches an acoustic wave. This process repeats at the repetition time of the pump optical pulses, every 50 ns. A rigorous model of this process is particularly challenging because the length and time scales of our measurements overlap with the fundamental length and time scales of the molecular mean-free path and molecular scattering times. The equations that describe the transport of heat and the propagation of the pressure disturbance will be linear because the temperature and pressure excursions are small, but linearity of the equations that describe the generation of the photoacoustic waves does not imply that these equations are local. In other words, we cannot be sure that the equations that relate temperature, pressure, and their derivatives depend on only a single point in space or that traditional approaches based on solutions of continuum differential equations[20] will be valid.

Because of these complexities and because the expertise of our research group is in experiment, not theory or computation, we have limited our modeling efforts to the development of an approximate continuum model for the generation of photoacoustic waves. This approximate model provides a context for the presentation of our data and an approximate means of interpreting the data in terms of various mechanisms that might contribute to the generation of photoacoustic waves. The model includes a finite thermal conductance of the gas−solid interface that reflects thermal accommodation at the gas−solid interface. Because of the approximate nature of the model, we cannot, at this time, provide precise values for thermal accommodation coefficients. We believe, however, that significant trends are apparent in the data and that the general approach we describe will yield quantitative data in the future as further research produces advances in both experiment and modeling.

Our approach for modeling the data is inspired by the work of Thomsen and co-workers[21] who studied the propagation of thermoelastically generated acoustic waves in solids using picosecond interferometry. Picosecond interferometry is a time-domain pump−probe measurement technique that is similar to our time-domain ellipsometry measurements; in both cases, the probe measures changes in the index of refraction of the medium, and the sensitivity of the probe to changes in index is periodic in the distance from an interface. Because of that spatial periodicity of the sensitivity function, the time-domain signal recorded by the probe is equivalent to measuring the Fourier amplitude of the variations in index at the spatial frequency of the sensitivity function.

In both types of experiments, picosecond interferometry and time-domain ellipsometry, a pressure disturbance propagates at the speed of sound v in the medium, and the time-domain signal oscillates with a frequency $\omega = (4\pi v \cos\theta)/\lambda$, where θ is the angle between the surface normal and the direction of the incident probe beam and λ is the optical wavelength in the medium. This frequency ω is the same as the frequency shift that is observed in inelastic light scattering; we therefore refer to ω as the Brillouin frequency.

Because the sensitivity of the probe to variations in index is limited to the response at the Brillouin frequency, we only need to model the generation of photoacoustic waves at the Brillouin frequency. In other words, instead of modeling the experiment in the time domain and then calculating the Fourier transform of the time-domain response and evaluating that Fourier transform at the Brillouin frequency, a simpler approach is to model the experiment directly in the frequency domain. In what follows, we first derive the frequency domain solution for the amplitude and phase of a photoacoustic wave generated by heat transfer from the solid surface with a periodic temperature. We then consider other mechanisms that can contribute to the photoacoustic wave. In the section on Experimental Details, we describe how heating of a metal thin film on a substrate by an ultrashort pump pulse gives rise to a broad spectrum of periodic surface temperatures in the frequency domain.

The generation of photoacoustic waves is typically calculated based on a moving piston model.[22,23] The amplitude of the periodic pressure oscillations p created by an oscillating piston of displacement amplitude s is

$$p = i\omega\rho v s \tag{2}$$

where ρ is the mass density of the gas; ω is the angular frequency; and v is the sound velocity. For an ideal gas, $v = (\gamma k_B T/m)^{1/2}$, where m is the molecular mass and γ is the specific heat ratio $\gamma = c_p/c_v$. Our ellipsometry measurements are sensitive to changes in the density of the gas, $\delta n = p/(\gamma k_B T)$. Combining terms gives

$$\frac{\delta n}{n} = \frac{i\omega s}{v} \tag{3}$$

The leading factor of i indicates that the change in density δn leads the displacement s by a phase factor $\pi/2$. (The maximum in the density occurs when the velocity of the piston is at a maximum; the maximum displacement of the piston occurs at 1/4 of a cycle later in time.) Our experiments probe photoacoustic waves at the Brillouin frequency for a fixed angle, $\omega = (4\pi v \cos\theta)/\lambda$, where λ is the optical wavelength. This geometrical constraint fixes the ratio ω/v.

$$\frac{\delta n}{n} = \frac{i4\pi s}{\lambda}\cos\theta \tag{4}$$

Equation 4 shows that the signal measured by ellipsometry normalized by the molecular density, or equivalently the pressure, is proportional to the displacement s. The phase of the ellipsometry signal leads the phase of the displacement by 90°.

We consider three mechanisms that can contribute to the displacement s: (i) thermal expansion of the gas; (ii) desorption of physisorbed gas molecules from the surface of the substrate; and (iii) thermal expansion of the substrate.

a. Thermal Expansion of the Gas. We make the approximation that the thermal effusivity of the gas is negligible in comparison to the effusivity of the substrate and assume that there is a non-negligible interfacial thermal resistance between the solid and gas; i.e., we assume that the thermal conductance of the solid−gas interface G is finite. Because the lateral

dx.doi.org/10.1021/jp302726u | J. Phys. Chem. C 2012, 116, 10896−10903

dimension of the heat source is large compared to the thermal penetration depth, heat flow is approximately one-dimensional in the distance from the interface z. The temperature field in the gas is

$$\delta T_g(z) = \frac{G}{G + \sqrt{i\omega\Lambda_g c_p}} \exp(q_g z)\delta T_s \quad (5)$$

δT_s is the complex amplitude of the temperature oscillations at the surface of the substrate, and q_g is the inverse of the thermal wavelength in the gas, $q_g = (i\omega c_p/\Lambda_g)^{1/2}$. Λ_g is the thermal conductivity of the gas, and c_p is the heat capacity per unit volume of the gas at constant pressure.

The displacement s_g created by the thermal expansion of the gas is the integral of the temperature field times the volume thermal expansion coefficient of the gas.

$$s_g = \sqrt{\frac{\Lambda_g}{i\omega c_p}} \frac{G}{G + \sqrt{i\omega\Lambda_g c_p}} \frac{\delta T_s}{T} \quad (6)$$

We simplify this equation using microscopic parameters that describe the kinetics of the gas: the mean thermal velocity $\bar{v}$ and the collision time τ. $G = (\gamma + 1)c_v\bar{v}\alpha/8$; for monatomic gases, $G = (1/3)c_v\bar{v}\alpha$. α is the thermal accommodation coefficient. For monatomic gases, $\Lambda = (1/3)c_v\bar{v}^2\tau$. Combining these relationships yields

$$s_g = \frac{\bar{v}\tau}{\sqrt{i3\gamma\omega\tau}} \frac{\alpha}{\alpha + \sqrt{i3\gamma\omega\tau}} \frac{\delta T_s}{T} \quad (7)$$

We convert this result to a contribution to $\delta n/n$ using eq 3. Making the approximation $(8/3\pi)^{1/2} \approx 1$, we obtain

$$\frac{\delta n}{n} = \frac{\alpha\sqrt{i\omega\tau}}{\alpha + \sqrt{i3\gamma\omega\tau}} \frac{\delta T_s}{\gamma T} \quad (8)$$

Equation 8 shows that the photoacoustically generated acoustic waves in the gas are sensitive to the thermal accommodation coefficient α when $(3\gamma\omega\tau)^{1/2} \geq \alpha$. In the limit of $(3\gamma\omega\tau)^{1/2} \gg \alpha$, the amplitude of the acoustic wave amplitude is proportional to α.

b. Gas Desorption and Adsorption. If the substrate is covered by adsorbed molecules, changes in the substrate temperature create changes in the equilibrium coverage and therefore changes in the gas density near the surface. The displacement s_{des} created by this mechanism will be approximately

$$s_{des} = \frac{1}{n} \frac{1}{(1 + i\omega\tau_{des})} \frac{\partial\theta}{\partial T} \delta T_s \quad (9)$$

where θ is the areal density of absorbed molecules. We have added a kinetic term involving a time scale τ_{des} to take into account the fact that the surface coverage cannot respond instantaneously to changes in the substrate temperature.

c. Thermal Expansion of the Substrate. In our experiments, the substrate is a thin metal film deposited on a sapphire wafer. Heating of the film and the sapphire wafer creates thermal expansion, and the displacement of the surface contributes to the generation of the acoustic wave.[24] A quantitative solution for the surface displacement in this geometry is available but complicated.[25] Here, we require only an estimate to show that the thermal expansion of the substrate produces a negligible contribution to s. The coefficient of thermal expansion α_{exp} of the metal film is larger than the thermal expansion coefficient of the sapphire wafer, and therefore s will be determined by the heating of the metal film if we assume that heat transfer from the film to the substrate is not too important at high frequencies. The temperature field in the metal film is uniform because the thermal diffusion coefficient of the metal film is high. The temperature oscillations of the film are

$$\delta T_s = \frac{J_0}{i\omega h c_f} \quad (10)$$

where J_0 is the amplitude of the period heat flux, c_f the heat capacity per unit volume of the metal film at constant pressure, and h the film thickness. Neglecting contributions from long-range elastic deformation of the substrate,[25] the displacement s is given by the temperature multiplied by the linear thermal expansion coefficient α_{exp}, the film thickness, and a term involving the Poisson ratio, ν.

$$s_{sub} = h\alpha_{exp}\frac{1 + \nu}{1 - \nu}\delta T_s \quad (11)$$

which can be compared to eq 7. In our experiments, the prefactor of δT_s in eq 11 is ≈2 pm/K. The corresponding term in eq 7 is on the order of the mean-free path divided by T, ~300 pm/K, for Ar at a pressure of 1 atm. Thus, we conclude that the thermal expansion of the metal film makes a negligible contribution to the photoacoustic signals.

III. EXPERIMENTAL DETAILS

A schematic diagram of the sample structure and the optical layout is shown in Figure 1. Heat pulses are produced by the absorption of the pump beam in a thin film of Ti deposited by electron-beam evaporation on a sapphire substrate. To minimize the thermoreflectance signal generated by the heat source and provide a surface with better defined chemistry, a thin film of Au is deposited on top of the Ti layer without exposure to air. The thicknesses of the Au (≈ 40 nm) and Ti (≈ 10 nm) layers are measured by Rutherford backscattering spectrometry in the Center for Microanalysis of Materials at the University of Illinois.

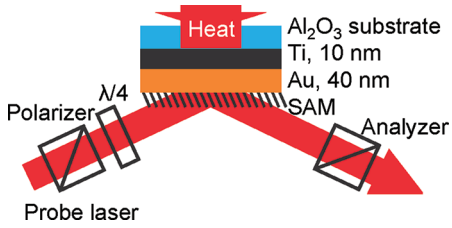

Figure 1. Schematic diagram of the experimental geometry. A pump optical pulse passes through the back-side of a transparent sapphire substrate and heats a thin metal film of Ti that is coated with Au. Heat flow from the surface of the Au layer into the adjacent gas is probed by off-null time-resolved ellipsometry.

The Au surfaces are either left bare or coated by one of two alkane-thiols to form self-assembled monolayers. Bare Au surfaces are prepared by plasma cleaning (Harrick, PDC-23G) for 10 min using 100 mTorr of O_2 and 20 W of rf power. Monolayers of 1-octadecanethiol (ODT) or 11-mercapto-undecanoic acid (MUA) are assembled on the surface of the Au film using conventional thiol chemistry to prepare a hydrophobic or hydrophilic surface, respectively. The Au thin

dx.doi.org/10.1021/jp302726u | J. Phys. Chem. C 2012, 116, 10896−10903

film sample is immersed in 1 mM concentration of the thiol dissolved in ethanol. After 24 h, the sample is rinsed with a mixture of 10 mL of ethanol and 1 mL of 1% HCl aqueous solution and subsequently rinsed with pure ethanol several times to remove thiols with nonspecific adsorption. Residual solvent is removed by blow drying with nitrogen gas. The prepared sample is stored in a vacuum and is used within one week. Contact angles of water are 111° for the hydrophobic surface and 37° for the hydrophilic surface.

Time-resolved ellipsometry[19] is used to measure the resulting time-dependent change of the phase Δ between $\hat{p}$ and $\hat{s}$ polarized light at variable time delays of the probe optical pulses relative to the pump pulses. Pump and probe pulses are generated by separate Ti:sapphire laser oscillators that coexist in a custom-built two-cavity laser setup; variable time delays between pump and probe pulses are generated by the small differences of the repetition rates of the two oscillators. (The repetition rates of the two mode-locked lasers are ≈19 MHz.) The two lasers operate at the same center wavelength, 790 nm.

The $1/e^2$ intensity radius of the focused pump beam is $w_0 \approx 15\ \mu$m. The shape of the probe beam on the surface of the sample is highly elongated because of the glancing angle of incidence; the $1/e^2$ intensity radii of the focused probe beam in the two directions are 7 and 18 μm. For the pump laser power of 70 mW, the temperature rise created by one pump pulse is ≈20 K, and the steady-state temperature rise created by the average laser power is ≈13 K. The volume probed is the region of overlap between the incident and reflected probe beam; this region extends 3−4 μm from the surface when the angle of incidence is 73−75°.

We use off-null ellipsometry with a polarizer−compensator−sample−analyzer arrangement to reduce background and improve the signal-to-noise ratio. We first create a null by adjusting the orientations θ of the polarizer and analyzer and then move off the null by offsetting the polarizer angle θ_P by ≈5°. The resulting angles are $\theta_P = 88.0°$ and $\theta_A = 47.8°$. Under these conditions, incident probe light is approximately circularly polarized. Differential detection using a reference beam is used to improve upon the limited dynamic range of the 100 MHz analog-to-digital data acquisition board used to detect each probe pulse. Typically 2000 probe pulses are averaged at each 100 fs of delay time. The total measurement time is typically 100 s. We have previously described[19] the approach we use to convert the changes in the intensity of the reflected probe beam to the changes in the ellipsometry angle Δ.

Our approach uses time-resolved ellipsometry signals to probe acoustic waves in the gas, but changes in the temperature of the Au/Ti film also produce a background change in the ellipsometry angle Δ that must be subtracted from the data (see Figure 2). The background signal is measured by evacuating the sample cell. The small and abrupt changes in Δ at short times are created by the longitudinal acoustic waves that are generated by the thermal expansion of the Ti and Au films. The largest temperature excursion occurs at $t \approx 200$ ps because the finite thermal conductance of the Ti/Au interface impedes the transfer of heat from the Ti layer to the surface layer of Au. At $t > 600$ ps, the temperature of the Au film decays as heat moves from the Au/Ti layers into the sapphire substrate.

Panels (b) and (c) of Figure 2 show the results of a Fourier analysis of the time domain response shown in (a). For a single, semi-infinite layer heated from the surface, the expected response in the frequency domain is an amplitude that scales with $\omega^{-1/2}$ and a constant phase of −45°. The heat capacity of the Au/Ti layers and the thermal conductance of the Au/Ti and Ti/sapphire interfaces cause a slightly stronger frequency dependence for the amplitude and a more substantial shift in the phase. The dashed lines in (b) and (c) are calculated using an approximate model.

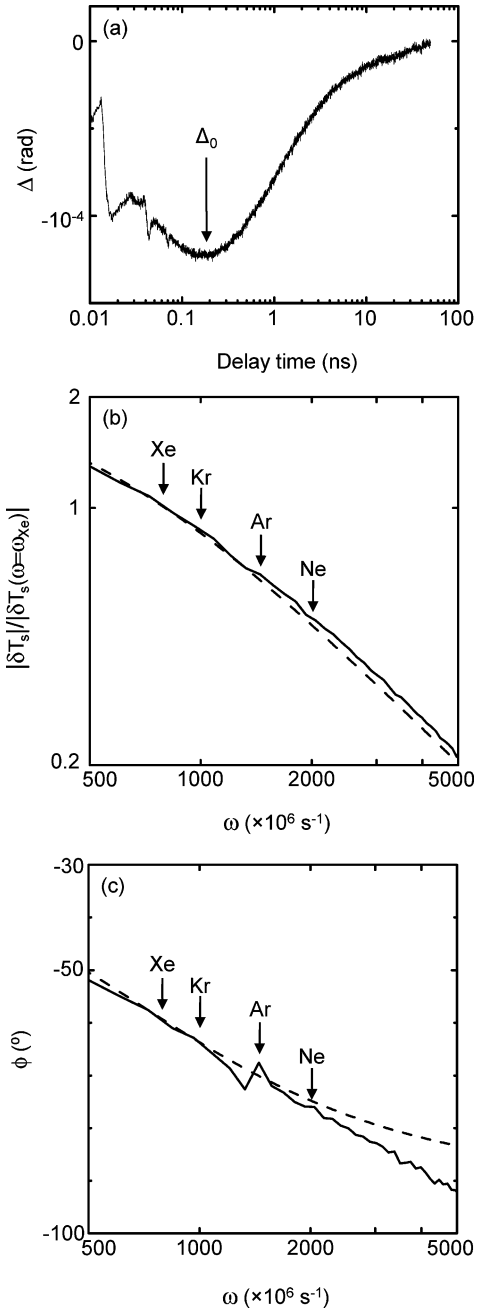

Figure 2. (a) Change in the ellipsometry angle Δ as a function of delay time measured in vacuum; Δ is proportional to the change in the temperature of the Au film. Panels (b) and (c) show the Fourier analysis of the time-domain response shown in panel (a). The Brillouin frequencies of the inert gases between Xe and Ne for our experimental geometry are marked by arrows. In (b), the amplitudes of the Fourier components of the surface temperature $|\delta T_s|$ are normalized by the amplitude of the Fourier component at the Brillouin frequency of Xe. The phase of $\delta T(\omega)$ is shown in panel (c). The dashed lines in (b) and (c) are the prediction of eq 12 using G_f = 80 MW m^{-2} K^{-1}.

dx.doi.org/10.1021/jp302726u | J. Phys. Chem. C 2012, 116, 10896−10903

$$\delta T_s = \frac{J_0}{G_f(\beta + i\omega\tau_f)} \qquad \beta = \frac{\sqrt{i\omega\Lambda_s c_s}}{G_f + \sqrt{i\omega\Lambda_s c_s}} \tag{12}$$

where Λ_s is the thermal conductivity of sapphire; c_s is the heat capacity per unit volume of sapphire; c_f is the average heat capacity per unit volume of the Au/Ti layer; G_f is the effective thermal conductance of the interface between the Au/Ti layer and the sapphire substrate; $\tau_f = hc_f/G_f$ is a characteristic time scale for the cooling of the metal film; and h is the thickness of the Au/Ti layer. The dashed lines in Figure 2b and 2c are calculated using $G_f = 80$ MW m^{-2} K^{-1}.

IV. RESULTS

A. Inert Gases at Bare and Alkane-thiol (Odt) Coated Au Surfaces. With an inert gas in the cell, heat transfer from the substrate to the gas causes the gas to expand and generates a change in density that propagates away from the substrate surface with the speed of sound. The change in density δn produces a change in the ellipsometry angle Δ. The sensitivity of Δ to δn is a periodic function of the distance from the surface z. Approximately, $\Delta \propto \delta n \cos(kz + \phi_s)$ where $k = 4\pi \cos\theta/\lambda$ is the spatial frequency of the sensitivity function, and ϕ_s is the phase of the sensitivity function. In our experiments, the angle of incidence is $\theta = 75°$, and the optical wavelength of the probe is $\lambda = 790$ nm; therefore, $k \approx 4.1\ \mu$m^{-1}. The value of ϕ_s depends on the complex index of refraction of the Au film, the exact value of θ, and the choices of the polarizer and analyzer angles. We calculate $\phi_s \approx 219°$ using Jones matrix formalism.[19]

Example data for the time evolution of Δ are plotted in Figure 3. The background signal (see Figure 2a) has been subtracted. The size of the signal is comparable to the peak change in Δ created by the changes in temperature of the Au film; therefore, the amplitude of the oscillations in Δ/Δ_0 created by the propagation of the density disturbance is on the order of unity.

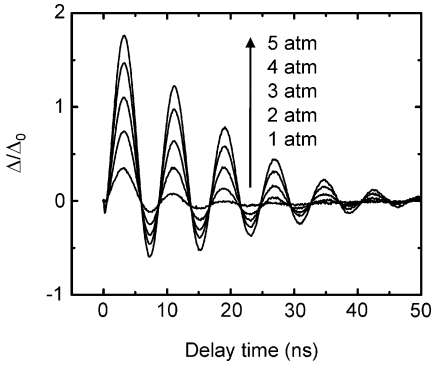

Figure 3. Changes in the ellipsometry angle Δ plotted as a function of delay time following heating of the substrate by the pump optical pulse. The gas is Xe gas at pressures between 1 and 5 atm. The changes in Δ are normalized by the peak change in ellipsometry angle Δ_0 measured in vacuum (see Figure 2a).

We have previously described[19] how we analyze these oscillatory signals to extract the amplitude and phase of the oscillations. The amplitudes of the oscillations are further normalized by $(n_{gas} - 1)$ where n_{gas} is the index of refraction of the gas. (We use tabulated data for n_{gas} at one atmosphere and assume that $(n_{gas} - 1)$ scales linearly with pressure. $(n_{gas} - 1) = 6.1 \times 10^{-5}$, 2.6×10^{-4}, 3.9×10^{-4}, and 6.4×10^{-4} at 295 K for Ne, Ar, Kr, and Xe.) The result is plotted in Figure 4a.

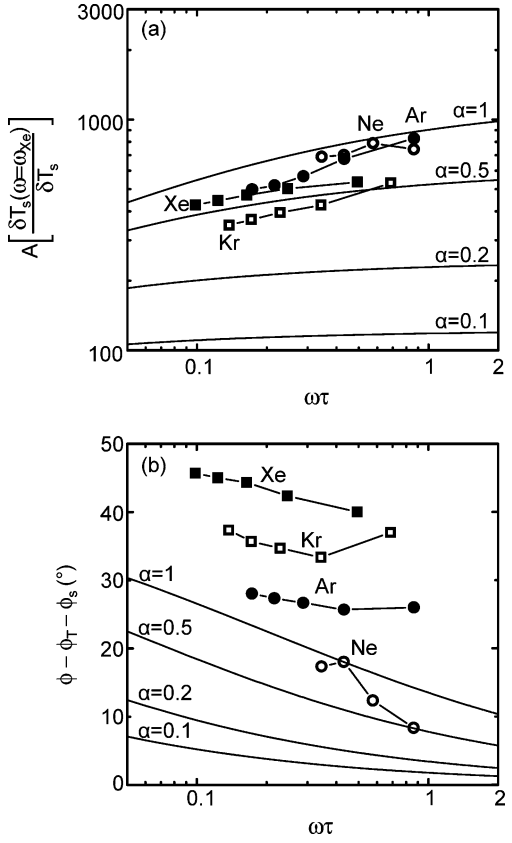

Figure 4. (a) Amplitude and (b) phase of the normalized photoacoustic signals A for inert gases interacting with bare Au surfaces plotted as a function of $\omega\tau$ where ω is the Brillouin frequency and τ the collision time for each gas. In (a), data for the relative changes in the ellipsometry angle of the type shown in Figure 3 have been normalized by $(n_{gas} - 1)$ where n_{gas} is the index of refraction of each gas. The signals are also scaled by the amplitude of the temperature oscillations at the Brillouin frequency of each gas to facilitate comparisons with the model. In (b), the measured phase ϕ is corrected by the phase of the temperature oscillations ϕ_T and the phase of the ellipsometry sensitivity function ϕ_s. Solid lines show the predictions of eq 8 for various values of the thermal accommodation coefficient α. For each gas except Ne, the data points are, from left to right, for pressures of 5, 4, 3, 2, and 1 atm. For Ne, the pressures are 5, 4, 3, and 2 atm.

To facilitate comparison with the prediction of the model, the prediction of eq 8 is scaled along the y-axis by amplitude of the temperature oscillations at the Brillouin frequency of each gas and a constant of proportionality that is fixed for all of the data shown in this paper. In other words, one free parameter, the constant of proportionality, is common for all data sets. The value of this free parameter depends on the energy density absorbed from the pump beam and sensitivity of the intensity of the probe to changes in index of refraction. The pump fluence and probe sensitivity can be estimated but not accurately enough to adequately constrain the free parameter. Ideally, we would use a reference sample with a well-understood response and use that reference sample to determine the value of the free parameter. We have not yet been able to create such a reference, however, and choose the free parameter so that the pressure dependence of the

dx.doi.org/10.1021/jp302726u | J. Phys. Chem. C 2012, 116, 10896−10903

amplitude is as consistent as possible with the model and that the largest signals are bounded by $\alpha = 1$.

The phase of the oscillations provides an additional comparison between the experiment and the continuum model. We adjust the measured phase to take into account the additional phase shift ϕ_t that is created by the finite thermal relaxation time of the Au/Ti metal films on the sapphire substrate (see Figure 2c). If we assume that our analysis of the amplitude data is accurate, the phase measured in the experiment leads to the phase predicted by the model by 0−20°. (We are not proposing that $\alpha > 1$ and are instead concluding that the model does not accurately describe the phase.) A closer examination of the data in Figure 4 reveals a discrepancy in the ordering of the data: the amplitude data for Xe lie below data for Ar and Ne, toward the direction expected for smaller α, but the phase data for Xe lie above data for the lighter mass atoms, in the direction expected for larger α. (We might expect that for bare Au α would increase in the series Ne, Ar, Kr, Xe because the mass of Xe is closest to the mass of Au.[8,18]) We do not yet understand the cause of these discrepancies and can only speculate at this time that the continuum model fails to accurately describe the acoustic wave generation when $\omega\tau$ is not small compared to 1, a physically reasonable finding. We also note that the Au surface may have a significant coverage of adsorbed atoms, particularly for the case of Xe.[9] Data for Ne show large deviations from the behavior of the higher mass gases because of systematic errors created by the small strength of the Ne photoacoustic signals and the strong damping of the acoustic waves at large values of $\omega\tau$.

These comparisons between experiment and model are repeated in Figure 5 for Au terminated by a self-assembled monolayer of 1-octadecanethiol (ODT). The composition at the surface of the ODT layer is a CH_3 group. The amplitude and phase of the photoacoustic waves for the ODT coated surface are, in most cases, reduced compared to bare Au, suggesting that α is slightly smaller for the ODT-coated surface. This result is counter to expectations since the lower mass of the surface groups and the lower rigidity of the self-assembled monolayer are expected to increase energy accommodation.[14,15,18]

B. Tetrafluoroethane (R-134a) Interacting with Au Terminated by Hydrophobic and Hydrophilic Self-Assembled Monolayers. The thermal accommodation of the vapor of a working fluid places an ultimate upper limit on the rate of heat transfer at the surface of a condenser. Figure 6 shows that the amplitude of photoacoustic waves generated by tetrafluoroethane (R-134a, a common refrigerant) interacting with Au terminated by hydrophobic (ODT) and hydrophilic (MUA) self-assembled monolayers differs by a factor of 2. The composition at the surface of the hydrophilic layer is a COOH group. We cannot, however, unambiguously associate the larger amplitude of the photoacoustic waves generated by the hydrophilic surface with a larger value of α because the phases of the photoacoustic signals for the two surfaces are similar and show even larger discrepancies with the model than we observe for the inert gases.

We consider the possibility that desorption of physisorbed molecules contributes to the generation of the acoustic wave. Since we do not have an independent measurement of temperature dependence of the surface coverage—i.e., we do not know the value of $d\theta/dT$ in eq 9—we can not reliably isolate the contributions to the photoacoustic signal from desorption and heat transfer. We can, however, make an order-

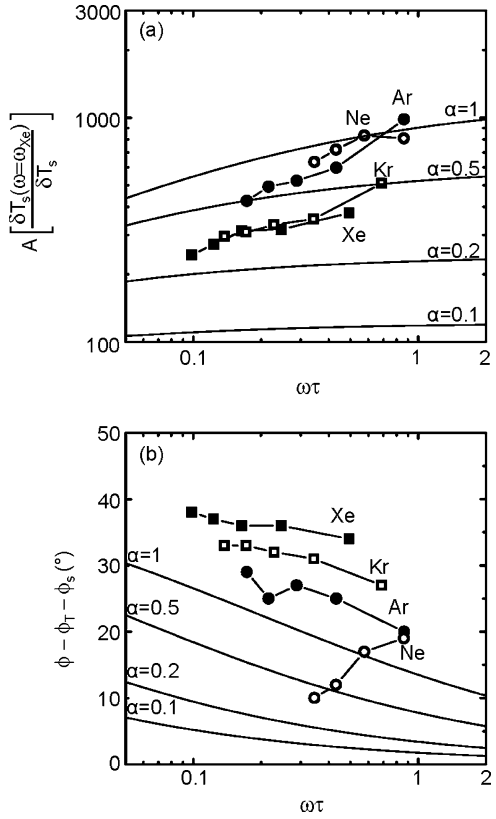

Figure 5. (a) Amplitude and (b) phase of the normalized photoacoustic signals A for inert gases interacting with Au coated by an alkane-thiol (ODT) self-assembled monolayer plotted as a function of $\omega\tau$ where ω is the Brillouin frequency and τ the collision time for each gas. Solid lines show the predictions of eq 8 for various values of the thermal accommodation coefficient α.

of-magnitude estimate of τ_{des} from the gas kinetics. Near equilibrium, the rate of desorption is equal to the rate of adsorption; the effect of the small temperature excursion is to increase the rate of desorption by a small amount so that the net coverage decreases to a new equilibrium value. If the sticking coefficient is close to unity, the rate of adsorption per unit area is $I = (1/4)n\bar{v}$. Inserting numbers for tetrafluoroethane, $I = 1.5 \times 10^{27}$ m^{-2} s^{-1} for R-134a at 40 °C and 1 atm, we estimate $\tau_{des} \approx 4$ ns and $\omega\tau \approx 4$. Therefore, we expect desorption to be slow on the time scale of the photoacoustic wave generation, and the phase of contribution of desorption to the signal should be close to 0°. Since the phase of the photoacoustic signals for tetrafluoroethane is ≈50°, similar to the phase for Xe interacting with bare Au, we conclude that desorption is not a significant contribution for tetrafluoroethane.

C. Ellipsometry Signals Created by Desorption of Methanol and Water. For completeness, we include data we have acquired using time-resolved ellipsometry for methanol vapor and water vapor interacting with Au terminated by hydrophobic (ODT) and hydrophilic (MUA) self-assembled monolayers. In both cases, $\omega\tau > 1$, and the acoustic waves are overdamped. For methanol, the ellipsometry signals essentially consist of a single peak at delay time ≈1.4 ns. The data plotted in Figures 7a and 7b show that the signal generated by hydrophilic surfaces is a factor of 3−4 larger than the strength of the peak for hydrophobic surfaces.

dx.doi.org/10.1021/jp302726u | J. Phys. Chem. C 2012, 116, 10896−10903

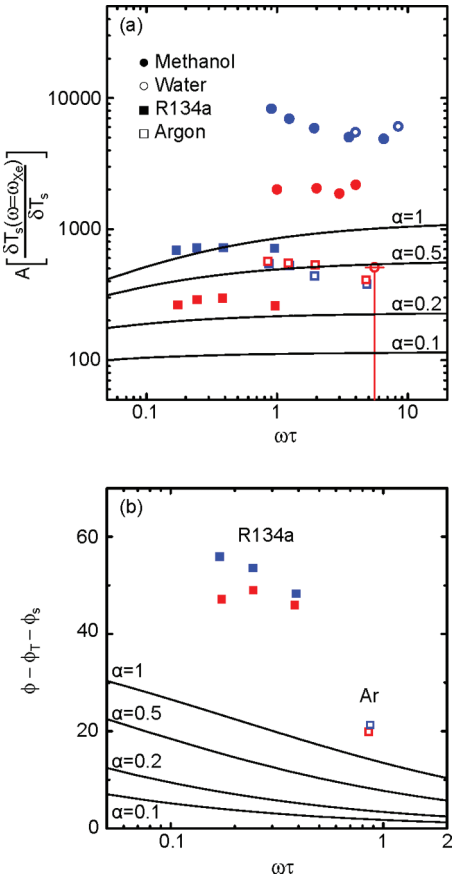

Figure 6. (a) Amplitude and (b) phase of the normalized photoacoustic signals A for tetrafluoroethane (R-134a) vapor (filled squares) and Ar (open squares) interacting with Au surfaces terminated by hydrophilic (MUA, blue symbols) and hydrophobic (ODT, red symbols) self-assembled monolayers. ω is the Brillouin frequency and τ the collision time for each gas derived from thermal conductivity data. Solid lines show the predictions of eq 8 for various values of the thermal accommodation coefficient α. The normalized peak value of the ellipsometry signals for methanol vapor (filled circles) and water vapor (open circles) are included for comparison. Since $\omega\tau > 1$ for methanol and water vapors, acoustic waves are overdamped and cannot be analyzed quantitatively. The red open symbol for water vapor interacting with the hydrophobic surface denotes an upper limit.

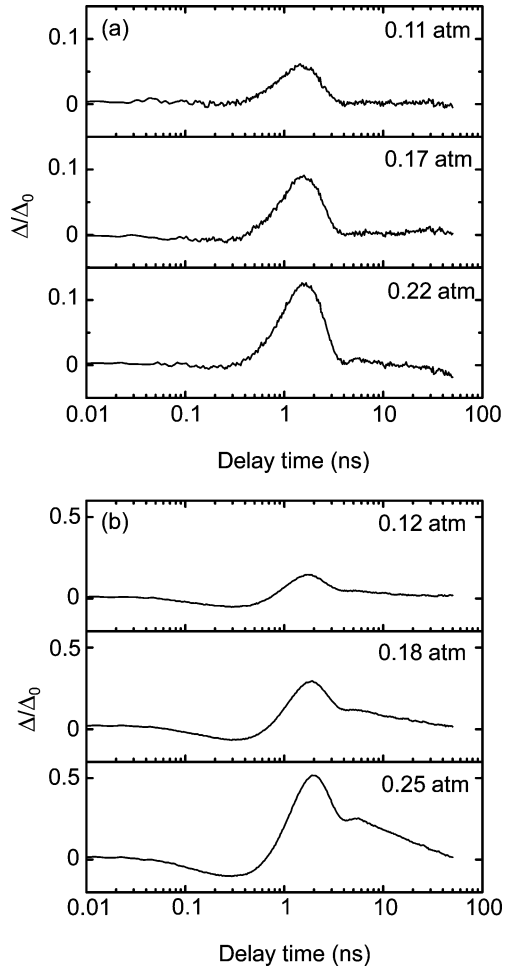

Figure 7. Changes in the ellipsometry angle Δ plotted as a function of delay time following heating of the substrate by the pump optical pulse. The gas is methanol vapor at pressures between 0.1 and 0.3 atm. The temperature is 40 °C . The changes in Δ are normalized by the peak change Δ_0 measured in vacuum (see Figure 2a). Panel (a) is for Au terminated by a hydrophobic self-assembled monolayer, and panel (b) is for Au terminated by a hydrophilic self-assembled monolayer.

We are not yet sure of the mechanisms that produce these signals. Both heat transfer (eq 8) and desorption (eq 9) could be contributing. We are not aware of any prior studies of the adsorption of methanol on self-assembled monolayers, but we can gain some insight from prior work on the adsorption of methanol on graphite[26] as a prototypical hydrophobic surface and ice[27] as a prototypical hydrophilic surface. A monolayer of methanol forms on graphite at a pressure of $P = 0.3P_0$ where P_0 is the saturated vapor pressure. (At 40 °C, P_0 = 0.35 atm for methanol and 0.075 atm for water.) A monolayer of methanol forms on ice at a pressure of only $P = 0.02P_0$. Our experiments span the range $0.1 < P/P_0 < 0.7$, and therefore both surfaces, hydrophobic and hydrophilic, are probably covered with at least some adsorbed methanol. The relatively large value of the normalized amplitudes (see Figure 6a) suggests that thermal desorption of methanol contributes significantly to the ellipsometry signal.

Because of the low molecular density at low pressures and the relatively small polarizability of H_2O at λ = 790 nm, signals generated by water vapor at $P < 0.1$ atm are small, and the signal-to-noise ratio is low. Figure 8 shows that the signal generated by a hydrophilic surface is easily detected, while the signal generated by a hydrophobic surface is comparable to the noise. Szór and co-workers have recently reported an extensive computational study of adsorption of water vapor on hydrophobic and hydrophilic self-assembled monolayers.[28] They found that the hydrophobic surface remained dry (essentially free of condensed water) up to the saturated vapor pressure P_0. A monolayer of water condenses at pressures $P \sim 10^{-3}P_0$ on a hydrophilic, OH-terminated surface. Therefore, we conclude that the signal for the hydrophobic surface is created by heat transfer, and the signal for the hydrophilic surface is most likely generated by thermal desorption of water from the surface.

V. DISCUSSION AND CONCLUSIONS

The principal conclusions of this study are 2-fold. First, the thermal accommodation coefficient, measured up to unprecedented high gas pressures, is shown to remain within a factor of 2−3 of unity. This conclusion is tempered by finding that continuum-based models fail to describe the data quantitatively,

dx.doi.org/10.1021/jp302726u | J. Phys. Chem. C 2012, 116, 10896−10903

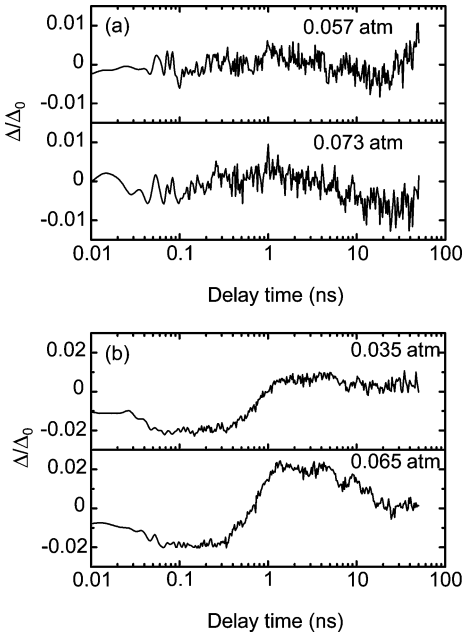

Figure 8. Changes in the ellipsometry angle Δ plotted as a function of delay time following heating of the substrate by the pump optical pulse. The gas is water vapor at pressures between 0.03 and 0.07 atm. The temperature is 40 °C. The changes in Δ are normalized by the peak change Δ_0 measured in vacuum (see Figure 2a). Panel (a) is for Au terminated by a hydrophobic self-assembled monolayer, and panel (b) is for Au terminated by a hydrophilic self-assembled monolayer.

as may be expected physically for problems where the mean-free path is comparable to the length scale of the experiment. Because of this limitation of the continuum model we are using to analyze our data, we are unable to derive quantitative values for the thermal accommodation coefficient α from our experiments. Nevertheless, the experiments are sensitive enough to reveal differences between α for different surface structures. The clearest example is tetrafluoroethane where the photoacoustic signals generated by a hydrophilic (MUA terminated) surface are a factor of 2 larger than the photoacoustic signals generated by a hydrophobic (ODT terminated) surface.

The characteristic time scale of our experiments, the inverse of the Brillouin frequency, 2−10 ns, is directly accessible to molecular dynamics (MD) simulations. We believe that comparisons between MD simulations of the generation of photoacoustic waves and the experimental data will enable us to derive quantitative values of α from experiment in the future.

Our data are consistent with other experiments and simulations that conclude that small values of the thermal accommodation, i.e., $\alpha < 0.3$, are relatively uncommon. The thermal accommodation coefficient for water vapor interacting with ice or liquid water surfaces has been constrained[1] to be $\alpha > 0.85$. A computational study of a gas interacting with carbon nanotubes[4] has shown that α approaches 1 when the interaction energy ε between the gas molecule and the surface is $\varepsilon > 4k_BT$. Extensive measurements of heat transfer[29] at low pressures, $P < 10$ Pa, indicate that for gases interacting with many common materials only for He gas is α significantly smaller than 1.

AUTHOR INFORMATION

Corresponding Author

*E-mail: d-cahill@illinois.edu.

Notes

The authors declare no competing financial interest.

ACKNOWLEDGMENTS

The authors gratefully acknowledge financial support through the Office of Naval Research MURI program (grant no. N00014-07-1-0723) and thank Dr. Dong-Wook Oh and Tamlin Matthews for measurements of film thickness by RBS.

REFERENCES

(1) Winkler, P. M.; Vrtala, A.; Wagner, P. E.; Kulmala, M.; Lehtinen, K. E. J.; Vesala, T. *Phys. Rev. Lett.* **2004**, *93*, 075701.
(2) Lu, J. W.; Alexander, W. A.; Morris, J. R. *Phys. Chem. Chem. Phys.* **2010**, *12*, 12533−12543.
(3) Burke, J. R.; Hollenbach, D. J. *Astrophys. J.* **1983**, *265*, 223−234.
(4) Hu, M.; Shenogin, S.; Keblinski, P. *Appl. Phys. Lett.* **2007**, *90*, 231905.
(5) Hsu, I.-K.; Pettes, M. T.; Aykol, M.; Shi, L.; Cronin, S. B. *Appl. Phys. Lett.* **2010**, *108*, 084307.
(6) Blodgett, K. B.; Langmuir, I. *Phys. Rev.* **1932**, *40*, 78−104.
(7) Eggleton, A. E. G.; Tomkins, F. C. *Trans. Faraday Soc.* **1952**, *48*, 738−749.
(8) Goodman, F. O.; Wachman, H. Y. *J. Chem. Phys.* **1967**, *46*, 2376.
(9) Tully, J. C. *Surf. Sci.* **1981**, *111*, 461−478.
(10) Arumainayagam, C. R.; Madix, R. J. *Prog. Surf. Sci.* **1991**, *38*, 1−102.
(11) Rettner, C. T.; Auerbach, D. J.; Tully, J. C.; Kleyn, A. W. *J. Phys. Chem.* **1996**, *100*, 13021−13033.
(12) Tully, J. C. *Annu. Rev. Phys. Chem.* **2000**, *51*, 153−158.
(13) Nathanson, G. M. *Annu. Rev. Phys. Chem.* **2004**, *55*, 231−55.
(14) Cohen, S. R.; Naaman, R.; Sagiv, J. *Phys. Rev. Lett.* **1987**, *58*, 1208−1211.
(15) Day, B. S.; Shuler, S. F.; Ducre, A.; Morris, J. R. *J. Chem. Phys.* **2003**, *119*, 8084.
(16) Isa, N.; Gibson, K. D.; Yan, T.; Hase, W.; Sibener, S. J. *J. Chem. Phys.* **2004**, *120*, 2417.
(17) Vázquez, S. A.; Morris, J. R.; Rahaman, A.; Mazyar, O. A.; Vayner, G.; Addepalli, S. V.; Hase, W. L.; Martínez-Núñez, E. *J. Phys. Chem. A* **2007**, *111*, 12785−12794.
(18) Alexander, W. A.; Day, B. S.; Moore, H. J.; Lee, T. R.; Morris, J. R.; Troya, D. *J. Chem. Phys.* **2008**, *128*, 014713.
(19) Min, C.-K.; Cahill, D. G.; Granick, S. *Rev. Sci. Instrum.* **2010**, *81*, 074902.
(20) Hu, H.; Zhu, T.; Xu, J. *Appl. Phys. Lett.* **2010**, *96*, 214101.
(21) Thomsen, C.; Grahn, H. T.; Maris, H. J.; Tauc, J. *Opt. Commun.* **1986**, *60*, 55−58.
(22) Rosencwaig, A.; Gersho, A. *J. Appl. Phys.* **1976**, *47*, 64.
(23) Tam, A. C. *Rev. Mod. Phys.* **1986**, *58*, 381.
(24) McDonald, F. A.; Wetsel, G. C. *J. Appl. Phys.* **1978**, *49*, 2313−2322.
(25) Zheng, X.; Cahill, D. G.; Weaver, R.; Zhao, J.-C. *J. Appl. Phys.* **2008**, *104*, 073509.
(26) Millard, B.; Beebe, R. A.; Cynars, J. *J. Phys. Chem.* **1954**, *58*, 468−471.
(27) Jedlovszky, P.; Pártay, L.; Hoang, P. N. M.; Picaud, S.; von Hessberg, P.; Crowley, J. N. *J. Am. Chem. Soc.* **2006**, *128*, 15300−15309.
(28) Szóri, M.; Jedlovszky, P.; Roeselová, M. *Phys. Chem. Chem. Phys.* **2010**, *12*, 4604−4616.
(29) Trott, W. M.; Castañeda, J. N.; Torczynski, J. R.; Gallis, M. A.; Rader, D. J. *Rev. Sci. Instrum.* **2011**, *82*, 035120.